

Novel Sr₂LuF₇-SiO₂ nano-glass-ceramics: structure and up-conversion luminescence

A.C. Yanes, J. del-Castillo, D. Luis, J. Puentes

Departamento de Física, Universidad de La Laguna, 38206 La Laguna, Tenerife, Spain

Abstract

Novel transparent nano-glass-ceramics comprising RE-doped Sr₂LuF₇ nanocrystals have been obtained by thermal treatment of precursor sol-gel glasses. The precipitated Sr₂LuF₇ nanocrystals with sizes from 4.5 to 11.5 nm, confirmed by X-Ray Diffraction and Transmission Electron Microscopy images, show a cubic phase structure. The luminescent features of Eu³⁺ ions, used as structural probes, evidence the distribution of RE ions into the fluoride nanocrystals. Under 980 nm laser excitation, intense UV, VIS and NIR up-conversion emissions were observed and studied in Yb³⁺-Tm³⁺, Yb³⁺-Er³⁺ and Yb³⁺-Ho³⁺ co-doped nano-glass-ceramics. These results suggest considering these nano-glass-ceramics for potential optical applications as high efficient UV up-conversion materials in UV solid state lasers, infrared tuneable phosphors and photonic integrated devices.

Novel Sr₂LuF₇-SiO₂ nano-glass-ceramics: structure and up-conversion luminescence

A.C. Yanes, J. del-Castillo, D. Luis, J. Puentes

Departamento de Física, Universidad de La Laguna, 38206 La Laguna, Tenerife, Spain

Abstract

Novel transparent nano-glass-ceramics comprising RE-doped Sr₂LuF₇ nanocrystals have been obtained by thermal treatment of precursor sol-gel glasses. The precipitated Sr₂LuF₇ nanocrystals with sizes from 4.5 to 11.5 nm, confirmed by X-Ray Diffraction and Transmission Electron Microscopy images, show a cubic phase structure. The luminescent features of Eu³⁺ ions, used as structural probes, evidence the distribution of RE ions into the fluoride nanocrystals. Under 980 nm laser excitation, intense UV, VIS and NIR up-conversion emissions were observed and studied in Yb³⁺-Tm³⁺, Yb³⁺-Er³⁺ and Yb³⁺-Ho³⁺ co-doped nano-glass-ceramics. These results suggest considering these nano-glass-ceramics for potential optical applications as high efficient UV up-conversion materials in UV solid state lasers, infrared tuneable phosphors and photonic integrated devices.

Keywords: nano-glass-ceramics, rare-earth ions, sol-gel technique, energy transfer, up-conversion.

Corresponding author: fjvargas@ull.edu.es

1. Introduction

Rare earth (RE)-doped up-conversion (UC) materials are a very important class of materials since they present a broad range of applications, such as infrared quantum counters detectors, temperature sensors, compact solid-state lasers, lighting and displays, solar cells, labelling, biomedical imaging and so on [1-11]. Among the up-converters RE ions, Tm^{3+} , Er^{3+} and Ho^{3+} have been extensively used due to their ladder-like energy levels structures, which introduce abundant energy levels into the gap of lattice host enabling photon absorption and subsequent energy transfer (ET) steps, giving rise to efficient UV, VIS and NIR emissions under low pump-power densities. Moreover, in order to further enhance the UC efficiency, these ions are often co-doped with Yb^{3+} ions, due to their large absorption cross-section in the 900-1100 nm NIR region, corresponding to the ${}^2\text{F}_{7/2} \rightarrow {}^2\text{F}_{5/2}$ transition, and a very efficient ET to these ions when they are very close in the host lattice. Additionally, compared to the co-doped RE ions, Yb^{3+} exhibit a reduced tendency for concentration-dependent quenching. Thus, very high Yb^{3+} concentrations can be used in order to increase their excitation probabilities.

Among RE-doped UC materials, RE-doped transparent oxyfluoride nanoglass-ceramics (nGCs) take advantage of the mechanical, thermal and chemical properties of oxide glass and the low phonon energy of fluoride environments that prevents non-radiative multiphoton relaxations. In this regard, RE doped-nGCs containing Y, La and Gd based-nanocrystals (NCs) have been extensively investigated [12-21], due to the facile incorporation of RE ions into the fluoride nanocrystalline phase (Y^{3+} , La^{3+} and Gd^{3+} ions can be easily substituted by RE^{3+} ions), which enhances the UC efficiency. On the other hand, RE-doped Lu-based fluorides, which present interest owing to their applications as scintillators, related to their high absorption cross-section for any kind of radiation [22-26], have received less attention. In particular, it should be noticed that there is only one report on RE doped- Sr_2LuF_7 systems which was ascribed to cubic structure [27]. Moreover, there are only few reports about Lu-based nGCs, which have been prepared by melt-quenching method. Thus, Guo et al. studied the luminescent properties of nGCs containing BaLuF_5 doped with Eu^{3+} [28] or Er^{3+} [29] ions, NaLuF_4 co-doped with Yb^{3+} - Tb^{3+} ions [30] and KLu_2F_7 doped with Er^{3+} [31].

1
2
3
4
5
6
7
8
9
10
11
12
13
14
15
16
17
18
19
20
21
22
23
24
25
26
27
28
29
30
31
32
33
34
35
36
37
38
39
40
41
42
43
44
45
46
47
48
49
50
51
52
53
54
55
56
57
58
59
60
61
62
63
64
65

Additionally, Chen et al. analysed the distribution of RE ions and the UC luminescence in nGCs containing Eu^{3+} doped- LuF_3 [32] and Yb^{3+} -($\text{Er}^{3+}/\text{Tm}^{3+}$) co-doped NaLuF_4 NCs [33], respectively. Therefore, in spite of the expensive lutetium raw materials and tough preparation [28-30], there is a growing interest in Lu-based nGCs as potential materials for scintillators [34] and also because they present excellent properties as up-conversion host matrix [26, 31, 33, 35]. In this respect, an alternative preparation procedure to obtain nGCs is through thermal treatment of precursor glasses obtained by sol-gel method. Besides its low cost, this method presents advantages such as its simplicity and precise control of the final composition [36] in comparison with conventional melting methods. Moreover, starting materials, in particular RE-dopant ions, can be mixed in the sol-gel method at molecular level, which improves the luminescence.

In this work we present for the first time RE doped nGCs containing Sr_2LuF_7 NCs, obtained from the sol-gel glasses. A complete structural analysis has been carried out, leading to the assignment of the Sr_2LuF_7 nanocrystalline phase as cubic. In order to analyse the incorporation grade of the RE dopant ions in the NCs, the Eu^{3+} ions were used as structural optical probes taken advantage of the hypersensitive character of the $^5\text{D}_0 \rightarrow ^7\text{F}_2$ transition, allowing us to discern between crystalline and glassy environments for RE ions. For nGCs co-doped with Yb^{3+} - Tm^{3+} , Yb^{3+} - Er^{3+} and Yb^{3+} - Ho^{3+} ions, intense UV, VIS and NIR UC emissions under 980 nm excitation were observed, and their corresponding ET mechanisms were described.

2. Experimental

Silica glasses have been prepared by sol-gel method, as described in ref. [20], with the following compositions: $95\text{SiO}_2\text{-}5\text{Sr}_2\text{LuF}_7$ doped with 0.1Eu^{3+} and co-doped with $1.0\text{Yb}^{3+}\text{-}0.1\text{Tm}^{3+}$, $1.0\text{Yb}^{3+}\text{-}0.1\text{Er}^{3+}$ and $1.0\text{Yb}^{3+}\text{-}0.1\text{Ho}^{3+}$. Tetraethoxysilane (TEOS) $\text{Si}(\text{OCH}_2\text{CH}_3)_4$, used as a source of SiO_2 , was hydrolysed for 1 h at room temperature with a mixed solution of ethanol and deionised H_2O , using acetic acid as a catalyst. The molar ratio of TEOS:ethanol: H_2O : CH_3COOH was 1:4:10:0.5. $\text{Sr}(\text{CH}_3\text{COO})_2$ and $\text{Lu}(\text{CH}_3\text{COO})_3 \cdot x\text{H}_2\text{O}$ were used as sources of Sr and Lu, respectively. The required quantities of $\text{Sr}(\text{CH}_3\text{COO})_2$, $\text{Lu}(\text{CH}_3\text{COO})_3 \cdot x\text{H}_2\text{O}$, $\text{Eu}(\text{CH}_3\text{COO})_3 \cdot x\text{H}_2\text{O}$, $\text{Yb}(\text{CH}_3\text{COO})_3 \cdot x\text{H}_2\text{O}$, $\text{Tm}(\text{CH}_3\text{COO})_3 \cdot x\text{H}_2\text{O}$, $\text{Er}(\text{CH}_3\text{COO})_3 \cdot x\text{H}_2\text{O}$ and $\text{Ho}(\text{CH}_3\text{COO})_3 \cdot x\text{H}_2\text{O}$ were dissolved in a CF_3COOH and H_2O solution and slowly mixed with the initial solution. The molar ratio of Sr^{2+} , RE (Lu^{3+} , Eu^{3+} , Yb^{3+} , Tm^{3+} , Er^{3+} , Ho^{3+}) ions to CF_3COOH was 2:1:7. In order to make the solution homogeneous it was stirred vigorously for 1 h at room temperature. A highly transparent gel was obtained by leaving the resultant homogeneous solution in a sealed container at $35\text{ }^\circ\text{C}$ for a week. The gels were then dried by slow evaporation for approximately four weeks to remove residual water and solvents. Finally, these sol-gel glasses were heat-treated in an air atmosphere up to $700\text{ }^\circ\text{C}$ in order to achieve the controlled precipitation of Sr_2LuF_7 nanocrystals required to produce transparent nGCs.

Powder X-ray diffraction (XRD) patterns of the samples were recorded with a Philips Panalytical X'Pert Pro diffractometer equipped with a primary monochromator, a $\text{Cu K}_{\alpha 1,2}$ radiation source, and an X'Celerator detector. The XRD patterns were collected with a step of 0.016° in the 2θ angular range from $15\text{-}90^\circ$ and an acquisition time of 2 h. Furthermore, the diffraction pattern of LaB_6 was used as an internal standard to calibrate the parameters of the instrumental profile. Transmission electron microscopy (TEM-HRTEM) images were obtained using a JEOL 2010F microscope operating at 200 kV, equipped with a Field Emission Gun, which allowed us to achieve a point-to-point resolution of 0.19 nm. Samples were prepared by dispersing fine powder, obtained by grinding the samples, in acetone and dropping them onto carbon-coated copper grids. Selected areas of the HRTEM images were mathematically filtered by means of Fast Fourier Transform (FFT) analysis resulting in Power Spectra patterns,

1
2
3
4
5
6
7
8
9
10
11
12
13
14
15
16
17
18
19
20
21
22
23
24
25
26
27
28
29
30
31
32
33
34
35
36
37
38
39
40
41
42
43
44
45
46
47
48
49
50
51
52
53
54
55
56
57
58
59
60
61
62
63
64
65

corresponding to the eigen-frequencies of the observed NCs. Furthermore, the relevant frequencies were selected to filter the noise in the zoomed areas of the HRTEM images and to produce higher contrast images of the atomic planes of the observed NCs.

Transmittance of nGCs was measured by means of a Perkin-Elmer Lambda 9 ultraviolet-visible-infrared (UV-VIS-IR) spectrophotometer with a resolution of 0.5 nm in the wavelength range of 320-850 nm.

Luminescence measurements were obtained by exciting the samples with light from a 75 W Xe arc lamp whose beam was directed through a 0.2 m monochromator (PTI spectrometer controlled by Felix32 software) and detected with a 0.2 m monochromator with a R928 photomultiplier. The time resolved photoluminescence measurements were carried out using a PTI spectrometer, where a 75 W Xenon flash lamp acts as excitation source. Moreover, UC measurements were carried out with a laser diode at 980 nm with a pump power up to 200 mW and a beam diameter of 2 mm, focused with a 50 mm lens and detected through a 0.2 m monochromator equipped with a photomultiplier. All spectra were collected at room temperature and corrected for the instrumental response. CCD digital camera was used to take colour pictures of UC luminescence emitted by the nGCs.

3. Results and Discussion

3.1 Structure and morphology

Structural characterization was carried out in terms of XRD patterns and TEM-HRTEM images. Fig. 1 shows the XRD curves of different nGCs with composition $95\text{SiO}_2\text{-}5\text{Sr}_2\text{LuF}_7\text{ RE}^{3+}$ -doped, heat-treated from 250 to 700 °C along with a precursor glass heat-treated at 200 °C. In the sample treated at 200 °C, only a broad diffraction band characteristic of SiO_2 in amorphous state is observed. However, in the samples treated from 250 °C to 700 °C, superposed to the broad amorphous band, diffraction peaks can be clearly distinguished at 27.0, 31.2, 44.9, 53.2, 55.7, 65.3, 72.0, 74.2 and 83.0° in the 2θ range from 15 to 90°, which correspond to the precipitation of Sr_2LuF_7 NCs in the cubic phase (fluorite structure, space group $Fm\text{-}3m$) [27]. It can be clearly seen that, when increasing the heat-treatment temperature, peaks become narrower and more intense, indicating a gradual growth and greater degree of crystallinity. Thus, by

1 using the Scherrer equation, from the width and position of diffraction peaks, mean NCs
2 sizes of 4.5, 6.0, 7.8, 8.8 and 11.5 nm are obtained for heat treatments at 250, 275, 300,
3 500 and 700 °C, respectively. These values are relatively smaller than those obtained by
4 L. Gong et al. [27], around 12-19 nm. Importantly, all nGCs present a high degree of
5 transparency due to the small NCs sizes, avoiding the scattering due to a mismatch of
6 the refractive index (see inset in Fig. 1).
7
8
9

10 In addition, RE-doped nGCs containing Sr₂LuF₇ NCs, heat-treated at 700 °C,
11 were characterized in terms of TEM and HRTEM images (see Fig. 2). In that respect,
12 Fig. 2a reveals well dispersed spherical NCs clearly distinguished over the gray
13 background in the TEM image, corresponding to the crystalline and the glassy phase,
14 respectively. The average nanoparticle size estimated from the TEM image is around 10
15 nm, in reasonably good agreement with the previous NC size calculated by the Scherrer
16 equation. Moreover, HRTEM image shown in Fig. 2b presents the detailed lattice
17 structure of a single precipitated Sr₂LuF₇ NC, which is indicative of a high degree of
18 crystallinity. The power spectrum of the FFT pattern obtained from the selected NC and
19 a higher contrasted image of this NC are also presented in the inset of Fig. 2b, obtained
20 by filtering the direct image by using the frequencies determined from the FFT pattern.
21 Lattice fringes can be clearly distinguished with an observed d-spacing of 2.1 Å, in
22 good agreement with the expected lattice spacing value for the (220) plane of Sr₂LuF₇
23 cubic phase by using the Bragg equation.
24
25
26
27
28
29
30
31
32
33
34
35

36 In order to investigate the distribution of the RE dopant ions in the nGCs
37 containing Sr₂LuF₇ NCs, the local environment of Eu³⁺ ions can be firstly analysed
38 taking into account their luminescent features as structural optical probe ion. Thus, Fig.
39 3 shows the emission spectra of Eu³⁺ doped samples heat-treated at indicated
40 temperatures, exciting at 392 nm, corresponding to the transition from the ⁷F₀ ground
41 level to the ⁵L₆ excited level. It can be clearly seen that the relative intensities and
42 spectral profiles strongly depend on the heat-treatment. For the sample heat-treated at
43 200 °C, only broad emission peaks at 580, 593, 613, 653 and 700 nm are observed,
44 related to transitions from ⁵D₀ to ⁷F_J (J=0-4) levels respectively, according to the energy
45 level diagram shown in the inset of Fig. 3. Moreover, the intensity ratio R of the
46 ⁵D₀→⁷F₂ transition to the ⁵D₀→⁷F₁ one [37], (very sensitive and insensitive to the local
47 symmetry surrounding Eu³⁺ ions, respectively), presents an R value of 4.3. Thus, both
48 results suggest that the Eu³⁺ ions should reside in a site with relatively high phonon
49 energy and low symmetry, without inversion centre, which can be related with a glassy
50
51
52
53
54
55
56
57
58
59
60
61
62
63
64
65

1 environment for Eu^{3+} ions, according to the results obtained by XRD measurements.
2 Similar spectral features are obtained for the sample heat-treated at 250 °C, but with a
3 smaller R value of 1.7 suggesting the incorporation of Eu^{3+} ions into the sites with
4 inversion symmetry in the face-centered cubic Sr_2LuF_7 NCs (around 5 nm size),
5 substituting the Lu^{3+} ions, with similar ionic radii and valence. For samples treated at
6 higher temperatures, a significant reduction in R is observed ($R \approx 0.5$), which is
7 consistent with nGCs comprising larger NCs (around 8-11 nm). In addition, emissions
8 coming mainly from upper energy level $^5\text{D}_1$ are also observed, showing higher
9 intensities for the nGCs treated at higher temperatures, which also supports the
10 progressive incorporation of Eu^{3+} ions into lower phonon energy environments of the
11 precipitates Sr_2LuF_7 NCs.
12
13
14
15
16
17
18
19

20 Furthermore, Fig. 4 shows the excitation and emission spectra of the Eu^{3+} doped
21 Sr_2LuF_7 nGCs heat-treated at 700 °C, by detecting and exciting at the indicated
22 wavelengths. The excitation spectra, by detecting at 592 and 616 nm, show the
23 characteristic excitation peaks of Eu^{3+} ions related with transitions from $^7\text{F}_0$ ground
24 level to the excited levels labelled in the figure (see energy level diagram in the inset of
25 Fig. 3). Although both excitation spectra seem to be very similar, when one looks
26 closer, it appears that the spectrum obtained by detecting the emission at 592 nm
27 (insensitive to the crystal field environment for the Eu^{3+} ions) presents narrower and
28 more resolved Stark components than those obtained by detecting at 616 nm
29 (hypersensitive to the crystal field and forbidden in the centrosymmetric environments).
30 This fact shows that an important fraction of the Eu^{3+} ions should be located into well
31 ordered Sr_2LuF_7 nanocrystalline environments. This assumption can be further
32 supported by the corresponding emission spectra. Thus, by site-selective excitation at
33 463 nm, a hypersensitive transition to the local structure around Eu^{3+} ions and therefore
34 forbidden in the centrosymmetric environments, the relative intensity of all emissions is
35 reduced when compared to those observed under excitation at 392 nm and, in particular
36 the emissions coming from upper-lying $^5\text{D}_{1-2}$ levels almost disappear. This can be
37 related to the remaining Eu^{3+} ions in the glassy phase and to those located at the
38 interface of the NCs, presenting higher phonon energies that prevent these emissions
39 from upper-lying levels. On the other hand, an R value of 0.5 was obtained when
40 exciting at 392 nm, which confirms that the environment of Eu^{3+} ions gets closer to a
41 centrosymmetric site, related to their distribution into the Sr_2LuF_7 NCs. As it is well-
42 known, the 392 nm excitation is not selective and equally excites all Eu^{3+} ions, so the R
43
44
45
46
47
48
49
50
51
52
53
54
55
56
57
58
59
60
61
62
63
64
65

1 value obtained is averaged over all sites and corresponds to a dominant contribution
2 from the volume NCs sites. On the contrary, by exciting at 463 nm, an R value of 1.6 is
3 obtained. This value is lower than the one obtained for the sample treated at 200 °C (R =
4 4.3) and those obtained, under the same excitation wavelength, for Eu³⁺ doped nGCs
5 previously studied by authors comprising KYF₄ (R= 3.3) [13] and YF₃ (R=4) [12] NCs
6 respectively. Accordingly, non-centrosymmetric environments for Eu³⁺ ions remaining
7 in the glassy phase and near the surface sites are assigned in this case.
8
9

10
11
12 In order to confirm the presence of an important fraction of Eu³⁺ ions inside the
13 Sr₂LuF₇ NCs, the photoluminescence decay curve of the ⁵D₀ level, exciting at 392 nm
14 and detecting the 593 nm emission was obtained, see inset in Fig. 4. The decay curve
15 shows a single exponential behaviour with a lifetime value of 9.3 ms, comparable to the
16 previously obtained values for the authors in similar nGCs systems [12,13,38], while the
17 short decay component ascribed to Eu³⁺ ions in the glassy phase was not observed,
18 showing that Eu³⁺ ions were distributed dominantly into the Sr₂LuF₇ NCs.
19
20
21
22
23
24
25
26

27 3.2 Up-conversion luminescence

28
29
30
31 Next, in order to take advantage of these new nGCs based on low phonon energy
32 Sr₂LuF₇ NCs, nGCs co-doped with Yb³⁺-Tm³⁺, Yb³⁺-Er³⁺ and Yb³⁺-Ho³⁺ ions, were
33 prepared and their UV, visible and NIR UC emissions under 980 nm excitation, were
34 studied.
35
36
37

38 Fig. 5 shows UC emission spectra of 1.0Yb³⁺-0.1Tm³⁺ (mol %) co-doped nGCs,
39 heat-treated at 700 °C, under 980 nm IR excitation and pump powers up to 200 mW. An
40 intense blue emission, visible to the naked eye, is observed even for pump power as low
41 as 25 mW. The visible UC spectra show the dominant blue emission, centered at 451
42 and 477 nm, along with a weaker red one, at around 650 nm, assigned to the ¹D₂→³F₄,
43 ¹G₄→³H₆ and ¹G₄→³F₄ transitions of Tm³⁺ ions, respectively. **The possible** mechanism
44 responsible for these emissions involves, first, the Yb³⁺ transition: ²F_{7/2}→²F_{5/2}, resonant
45 with the IR excitation. Next, subsequent efficient ET processes from Yb³⁺ to Tm³⁺ ions
46 populate Tm³⁺: ³H₅, ³F_{3,2} and ¹G₄ levels, involving 1, 2 and 3 photons, respectively,
47 while the ¹D₂ level **would correspond to** a 4-photon UC process, assisted by the cross
48 relaxation (CR) mechanism ³F_{3,2} + ³H₄ → ³H₆ + ¹D₂ of Tm³⁺ ions [8, 39-42] (see energy
49 level diagram in the right inset in Fig.5).
50
51
52
53
54
55
56
57
58
59
60
61
62
63
64
65

1
2
3
4
5
6
7
8
9
10
11
12
13
14
15
16
17
18
19
20
21
22
23
24
25
26
27
28
29
30
31
In addition, other UC emissions are also observed in the NIR and UV ranges of the spectra. On one hand, the emission at 802 nm, ascribed to ${}^3\text{H}_4 \rightarrow {}^3\text{H}_6$ transition, is achieved after non-radiative de-excitation from ${}^3\text{F}_{3,2}$ level. On the other hand, UV emissions at 362, 350 and 290 nm are assigned to ${}^1\text{D}_2 \rightarrow {}^3\text{H}_6$, ${}^1\text{I}_6 \rightarrow {}^3\text{F}_4$ and ${}^1\text{I}_6 \rightarrow {}^3\text{H}_6$ transitions respectively, where the upper excited level, ${}^1\text{I}_6$, can be efficiently populated by ET from Yb^{3+} ions by the channel $\text{Yb}^{3+}: {}^2\text{F}_{5/2} + \text{Tm}^{3+}: {}^1\text{D}_2 \rightarrow \text{Yb}^{3+}: {}^2\text{F}_{7/2} + \text{Tm}^{3+}: {}^1\text{I}_6$, (see right inset in Fig.5). It should be noticed that the emissions coming from these levels, ${}^1\text{D}_2$ and ${}^1\text{I}_6$, have not been previously observed in Yb^{3+} - Tm^{3+} co-doped Sr_2LuF_7 NCs [27]. It can also be seen that by increasing the pump power, high-energy UC emissions, from ${}^1\text{D}_2$ and ${}^1\text{I}_6$ levels, enhance faster than the other UC emissions. This fact implies that pump power density results critical in optimizing the population of higher energy levels and therefore in obtaining more efficient UC emissions, in particular in the UV range. Besides, a progressive change of the relative intensities in the UC emissions can be also observed, when increasing the heat-treatment temperature of these nGCs, from 300 to 700 °C (see left inset in Fig.5), showing a shortening of interionic distances, favouring the ET processes and thus enhancing the high energetic UC emissions.

32
33
34
35
36
37
38
39
40
41
42
43
44
45
46
47
48
49
50
51
52
53
Finally, in order to complete the luminescent study, UC spectra of 1.0Yb^{3+} - 0.1Er^{3+} and 1.0Yb^{3+} - 0.1Ho^{3+} co-doped nGCs heat-treated at 700 °C, were measured under 980 nm excitation at 200 mW pump power (see Fig.6(a) and (b) respectively). **Moreover, corresponding precursor glasses heat treated at 200 °C were measured under the same conditions, showing a luminescence practically negligible (not shown).** For the Yb^{3+} - Er^{3+} co-doped nGCs, the observed emission peaks at 407, 523-541 and 654 nm can be assigned to ${}^2\text{H}_{9/2} \rightarrow {}^4\text{I}_{15/2}$ (blue), ${}^4\text{S}_{3/2}({}^2\text{H}_{11/2}) \rightarrow {}^4\text{I}_{15/2}$ (green) and ${}^4\text{F}_{9/2} \rightarrow {}^4\text{I}_{15/2}$ (red) transitions of Er^{3+} ions (see energy levels diagram in the inset of Fig.6(a)). On the other hand, the corresponding UC emission spectrum of Yb^{3+} - Ho^{3+} co-doped nGCs presents red and green emissions, located at 540 and 650 nm, which are assigned to the ${}^5\text{S}_2({}^5\text{F}_4) \rightarrow {}^5\text{I}_8$ and ${}^5\text{F}_5 \rightarrow {}^5\text{I}_8$ transitions of Ho^{3+} ions respectively (see energy level diagram in the inset of Fig. 6(b)).

54
55
56
57
58
59
60
61
62
63
64
65
The UC mechanism in Yb^{3+} - Er^{3+} and Yb^{3+} - Ho^{3+} co-doped systems has been extensively investigated [20, 43]. Under 980 nm excitation, an initial ET from Yb^{3+} ions in the ${}^2\text{F}_{5/2}$ excited level to the Ho^{3+} or Er^{3+} ions, populates the ${}^5\text{I}_6$ and ${}^4\text{I}_{11/2}$ levels respectively. Next, a second ET from Yb^{3+} ions populates the corresponding emitting

1
2
3
4
5
6
7
8
9
10
11
12
13
14
15
16
17
18
19
20
21
22
23
24
25
26
27
28
29
30
31
32
33
34
35
36
37
38
39
40
41
42
43
44
45
46
47
48
49
50
51
52
53
54
55
56
57
58
59
60
61
62
63
64
65

levels (see insets in Fig.6), giving rise to intense red and green emissions in both co-doped nGCs systems, involving 2-photon processes. Moreover, in both cases the contribution of the green emission is dominant, as it is quantified by the CIE formalism [44], with corresponding colour coordinates (0.308;0.668) for $\text{Yb}^{3+}\text{-Er}^{3+}$ and (0.309;0.674) for $\text{Yb}^{3+}\text{-Ho}^{3+}$ co-doped nGCs, located near the border of the green region. Moreover, taking into account that the colour coordinates for the $\text{Yb}^{3+}\text{-Tm}^{3+}$ co-doped nGCs, also treated at 700 °C, are (0.183;0.106) located near the border of the blue region, it should be possible to generate white light through the adequate combination of Yb^{3+} , Tm^{3+} and Er^{3+} or Ho^{3+} ions doping level in the present Sr_2LuF_7 nGCs. Research along this line is currently being carried out.

Conclusions

A novel transparent Eu^{3+} -doped or $\text{Yb}^{3+}\text{-Tm}^{3+}$, $\text{Yb}^{3+}\text{-Er}^{3+}$ and $\text{Yb}^{3+}\text{-Ho}^{3+}$ co-doped nGCs containing cubic Sr_2LuF_7 NCs, confirmed by XRD and HRTEM images, were successfully developed by the sol-gel method and posterior thermal treatments. The use of Eu^{3+} as structural probe ion revealed different environments for RE ions and suggested that an important fraction of these ones are located into the nanocrystalline Sr_2LuF_7 phase. Main UV, VIS and NIR UC emissions were analysed in the $\text{Yb}^{3+}\text{-Tm}^{3+}$ co-doped nGCs as a function of pump-power and heat-treatment temperature. Green and red UC emissions were observed in $\text{Yb}^{3+}\text{-Er}^{3+}$ and $\text{Yb}^{3+}\text{-Ho}^{3+}$ co-doped nGCs and their corresponding ET mechanisms were described. **Results obtained suggest that these systems can be considered for potential optical applications as high efficient UV-VIS up-conversion materials in solid state lasers and photonic integrated devices.**

Acknowledgments

The authors would like to thank Fundación CajaCanarias (NAFOWLEDs) and Ministerio de Economía y Competitividad (MAT2014-57551-R (LUNALEDs) for their financial support. We also would like to thanks Mrs. Julia Troyano for her valuable contribution and suggestions.

References

1. S. Sivakumar, F. Veggel, P. May, *J. Am. Chem. Soc.* 129, 620 (2007).
2. X. Wang, J. Zhuang, Q. Peng, Y. Li, *Inorg. Chem.* 45, 6661 (2006).
3. G. De, W. Qin, J. Zhang, J. Zhang, Y. Wang, C. Cao, Y. Cui, *J. Solid State Chem.* 179, 955 (2006).
4. C. Cao, W. Qin, J. Zhang, Y. Wang, P. Zhu, G. Wei, G. Wang, R. Kim, L. Wang, *Opt. Lett.* 33, 857 (2008).
5. Q. Chen, X. Wang, F. Chen, Q. Zhang, B. Dong, H. Yang, G. Liu, Y. Zhu, *J. Mater. Chem.* 21, 7661 (2011).
6. Y. Liu, Y. Chen, Y. Lin, Q. Tan, Z. Luo, Y. Huang, *J. Opt. Soc. Am. B*, 24, 5, 1046 (2007).
7. F. Auzel, *Chem. Rev.* 104, 139 (2004).
8. D. Chen, Y. Wang, F. Bao, Y. Yu, *J. Appl. Phys.*, 101, 113511 (2007).
9. G. Blasse, B. C. Grabmaier, in *Luminescence Materials*; Springer-Verlag: Berlin, 195, (1994).
10. Y. Yu, Y. Wang, D. Chen, F. Liu, *Ceram. Inter.* 34, 2143 (2008).
11. J. F. Suyver, J. Grimm, M. K. van Veen, D. Biner, K. W. Krämer, H. U. Güdel, *J. Lumin.* 117 (2006).
12. A. C. Yanes, A. Santana-Alonso, J. Méndez-Ramos, J. del-Castillo, V. D. Rodríguez, *Adv. Funct. Mater.* 21, 3136 (2011).
13. A. C. Yanes, A. Santana-Alonso, J. Méndez-Ramos, J. del-Castillo, *Appl. Phys. B. Laser and Optics.* 113, 589 (2013).
14. D. Deng, S. Xu, S. Zhao, C. Li, H. Wang, H. Ju, *J. Lumin.* 129, 1266 (2009).
15. K.W. Krämer, D. Biner, G. Frei, H. U. Güdel, M.P. Hehlen, S.R. Lüthi, *Chem. Mater.* 16, 1244 (2004).
16. Z. Shan, D. Chen, Y. Yu, P. Huang, F. Weng, H. Lin, Y. Wang, *Mater. Res. Bull.* 45, 1017 (2010).
17. X. Qiao, X. Fan, M. Wang, H. Yang, X. Zhang, *J. Appl. Phys.* 104, 043508 (2008).
18. J. del-Castillo, J. Méndez-Ramos, A.C. Yanes, V. D. Rodríguez, *J. Nanopart. Res.* 11, 879 (2009).
19. H. K. Dan, D. Zhou, R. Wang, X. Yu, Q. Jiao, Z. Yang, Z. Song, J. Qiu, *Opt. Mater.* 36, 639 (2014).

- 1
2
3
4
5
6
7
8
9
10
11
12
13
14
15
16
17
18
19
20
21
22
23
24
25
26
27
28
29
30
31
32
33
34
35
36
37
38
39
40
41
42
43
44
45
46
47
48
49
50
51
52
53
54
55
56
57
58
59
60
61
62
63
64
65
20. A. Biswas, G. S. Maciel, C. S. Friend, P. N. Prasad, *J. Non-Cryst. Solids* 316, 393 (2003).
 21. X. Qiao, X. Fan, M. Wang, *Appl. Phys. Lett.* 89, 111919 (2006).
 22. J. Pejchal, K. Fukuda, S. Kurosawa, Y. Yokota, A. Yoshikawa, *Opt. Mater* (2014) In press.
 23. J. Lin, J. Huo, Y. Cai, Q. Wang, *J. Lumin.* 144, 5 (2013).
 24. L. G. Jacobsohn, C. J. Kucera, K. B. Sprinkle, S. A. Roberts, E. G. Yukihara, T. A. DeVol, J. Ballato, *IEEE Nucl. Sci. Symp. Conf.* 1600 (2010).
 25. L. Rao, W. Lu, T. Zeng, Z. Yi, H. Wang, H. Liu, S. Zeng, *Dalton Trans.* 43, 13343 (2014).
 26. S. Sarkar, B. Meesaragandla, C. Hazra, V. Mahalingam, *Adv. Mater.* 25, 856 (2013).
 27. L. Gong, M. Ma, C. Xu, X. Li, S. Wang, J. Lin, Q. Yang, *J. Lumin.* 134, 718 (2013).
 28. X. Liu, Y. Wei, R. Wei, J. Yang, H. Guo, *J. Am. Ceram. Soc.* 96, 3, 798 (2013).
 29. J. Yang, H. Guo, X. Liu, H. M. Noh, J. H. Jeong, *J. Lumin.* 151, 71 (2014).
 30. Y. Wei, X. Liu, X. Chi, R. Wei, H. Guo, *J. Alloys and Comps.* 578, 385 (2013).
 31. Y. Wei, X. Li, H. Guo, *Opt. Mater. Exp.* 4, 7, 1367 (2014).
 32. D. Chen, Y. Yu, P. Huang, Y. Wang, *Cryst. Eng. Comm.* 11, 1686 (2009).
 33. D. Cheng, Y. Zhou, Z. Wan, P. Huang, H. Yu, H. Lu, Z. Ji, *J. Eur. Ceram. Soc.* 2015 (In press).
 34. J. A. Johnson, S. Schweizer, B. Henke, G. Chen, J. Woodford, P. J. Newman, D. R. Macfarlane, *J. Appl. Phys.* 100, 3, 034701 (2006).
 35. S. Xiao, X. Yang, J. W. Ding, X. H. Yan, *J. Phys. Chem. C.* 111, 8161 (2007).
 36. C. J. Brinker, G. W. Scherer, *Sol-gel science: the physics and chemistry of sol-gel processing* (Academic Press, Boston, 1990).
 37. S. Cotton, Wiley, West Sussex, UK, pp.14 (Chapter 2).
 38. J. del-Castillo, A.C. Yanes, S. Abe, P.F. Smet, *J. Alloys and Comps.* 635, 136 (2015).
 39. C. Cao, W. Qin, J. Zhang, Y. Yang, P. Zhu, G. Wang, G. Wei, L. Wang, L. Jin, *J. Fluorine Chem.* 129, 204 (2008).
 40. W. Guofeng, Q. Weiping, W. Lili, W. Guodong, Z. Peifen, Z. Daisheng, D. Fuheng, *J. Rare Earths* 27, 330 (2009).
 41. D. Chen, Y. Wang, Y. Yu, P. Huang, *Appl. Phys. Lett.* 91, 051920 (2007).

1
2
3
4
5
6
7
8
9
10
11
12
13
14
15
16
17
18
19
20
21
22
23
24
25
26
27
28
29
30
31
32
33
34
35
36
37
38
39
40
41
42
43
44
45
46
47
48
49
50
51
52
53
54
55
56
57
58
59
60
61
62
63
64
65

42. H. Lin, D. Chen, Y. Yu, A. Yang, R. Zhang, Y. Wang. *Mater. Res. Bull.* 47, 469 (2012).

43. A. S. Gouveia-Neto, E. B. da Costa, L. A. Bueno, S. J. L. Ribeiro, *J. Lumin.* 110, 79 (2004).

44. CIE colorimetry (Official Recommendations of the International Commission on Illumination) CIE Publication, 15, 1971, CIE, Paris.

Figure captions

1
2
3
4 **Fig.1.** XRD patterns of RE³⁺ doped-Sr₂LuF₇ nGCs heat-treated at indicated
5 temperatures. Inset shows the transmittance curve of the transparent nGC heat-treated at
6 700 °C.
7
8
9

10
11 **Fig. 2.** (a) TEM and (b) HRTEM images of RE³⁺ doped-Sr₂LuF₇ nGCs heat treated at
12 700 °C. Inset shows the power spectrum (FFT pattern) and filtered higher-contrasted
13 image of the squared NC.
14
15
16

17
18 **Fig. 3.** Emission spectra of Eu³⁺ doped-Sr₂LuF₇ nGCs heat-treated at indicated
19 temperatures, exciting at 392 nm. All spectra have been normalized at 590 nm (⁵D₀→
20 ⁷F₁ transition). Energy levels diagram of Eu³⁺ ions is included in the inset.
21
22
23
24

25 **Fig. 4.** Excitation and emission spectra of Eu³⁺ doped-Sr₂LuF₇ nGCs heat-treated at 700
26 °C, detecting and exciting at indicated wavelengths. Excitation spectra have been
27 normalized at 525 nm (⁷F₀→⁵D₁ transition) and the emission spectra at their
28 corresponding maxima. Inset shows photoluminescence decay curve of this nGC,
29 excited at 392 nm, monitoring the 592 nm emission.
30
31
32
33
34

35 **Fig. 5.** UC emission spectra of 1.0Yb³⁺-0.1Tm³⁺ co-doped-Sr₂LuF₇ nGCs (mol%) heat
36 treated at 700 °C, under excitation at 980 nm, at indicated pump powers. Right inset
37 shows the energy level diagrams of Yb³⁺ and Tm³⁺ ions with main UC emissions and
38 corresponding population mechanisms. Left inset shows UC emission spectra of
39 1.0Yb³⁺-0.1Tm³⁺ co-doped-nGCs (mol%) heat-treated at indicated temperatures, under
40 excitation at 980 nm and 200 mW of pump power, **along with a photograph of the nGC**
41 **heat treated at 700 °C.** All spectra have been normalized at 802 nm (³H₄→³H₆
42 transition).
43
44
45
46
47
48
49
50

51 **Fig. 6.** UC emission spectra of (a) 1.0Yb³⁺-0.1Er³⁺ and (b) 1.0Yb³⁺-0.1Ho³⁺ co-doped-
52 nGCs (mol%) heat treated at 700 °C, under excitation at 980 nm and 200 mW of pump
53 power. Insets show the energy level diagrams of Er³⁺ and Ho³⁺ ions **and their**
54 **corresponding photographs.** Spectra have been normalized at their corresponding
55 maxima.
56
57
58
59
60
61
62
63
64
65

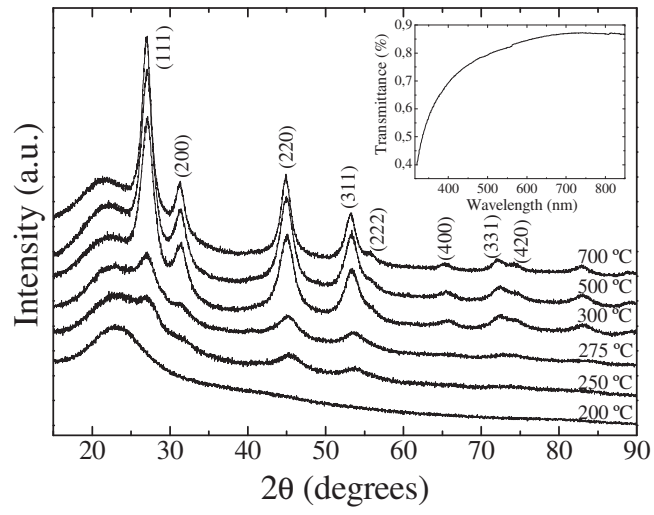


Fig. 1.

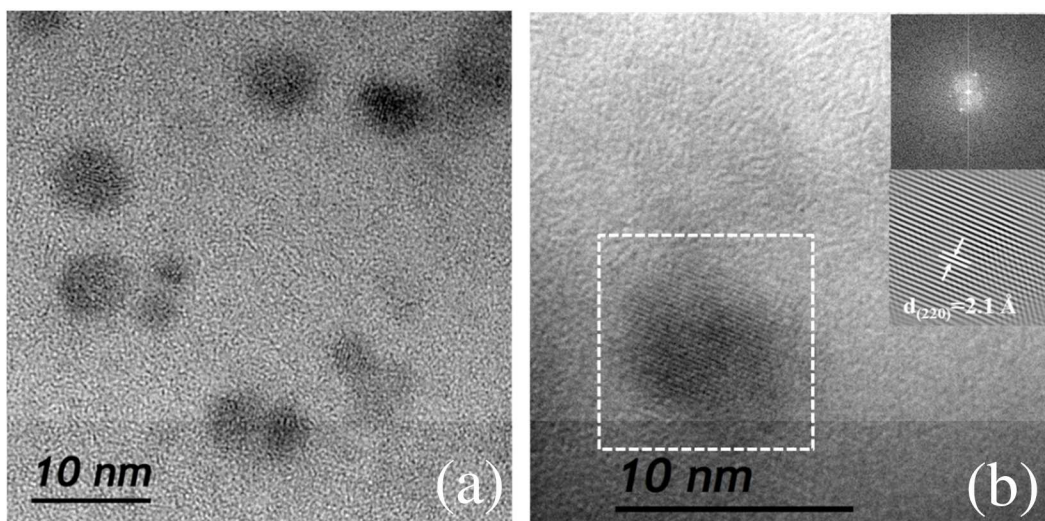


Fig. 2.

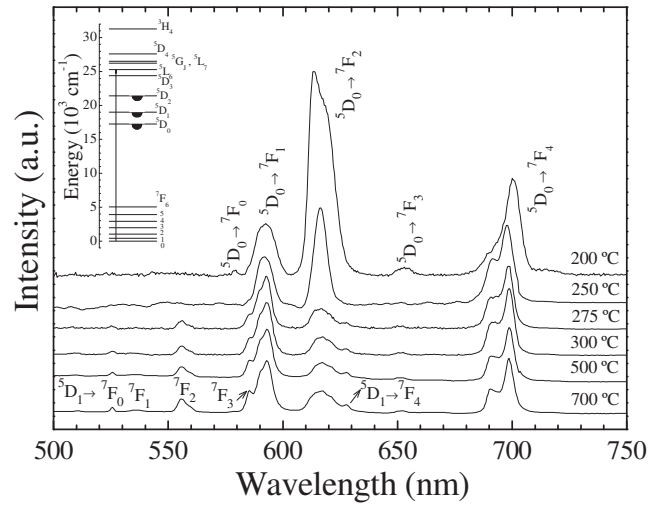


Fig. 3.

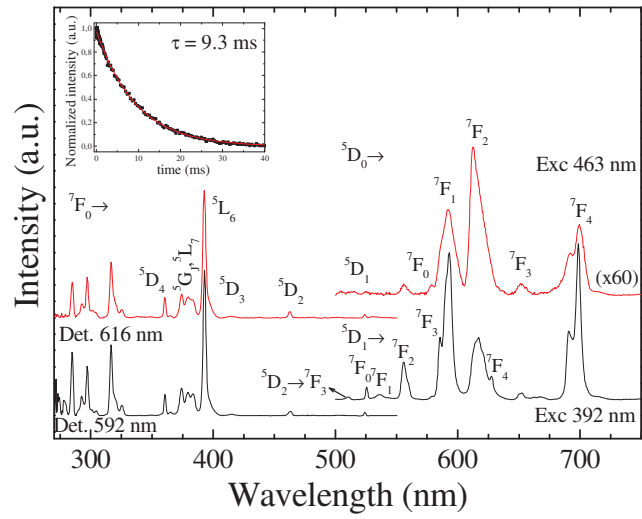
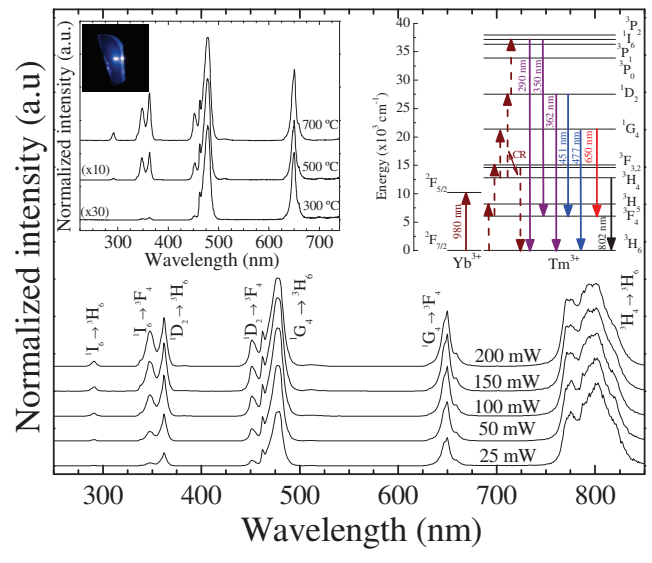


Fig. 4.

Figure



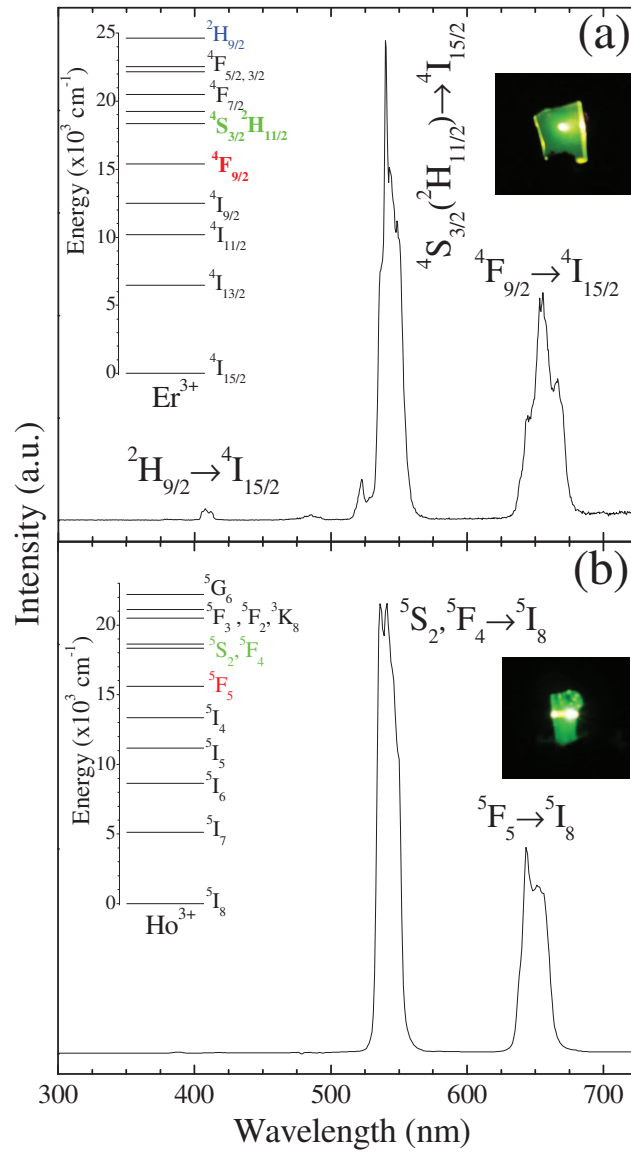


Fig. 6.